High-Pressure Behavior and Polymorphism of Titanium Oxynitride Phase $Ti_{2.85}O_4N$

Ashkan Salamat, Geoffrey Hyett, Raul Quesada Cabrera, Paul F. McMillan,* and Ivan P. Parkin*

Materials Research Centre, Christopher Ingold Laboratory, University College London, 20 Gordon Street, London, WC1H 0AJ, United Kingdom

Received: January 26, 2010; Revised Manuscript Received: March 18, 2010

We report a crystallographic study of $Ti_{2.85}O_4N$, a new titanium oxynitride phase discovered using chemical vapor deposition and combinatorial chemistry techniques, under high-pressure conditions. Synchrotron X-ray diffraction was used to monitor structural changes in the material during compression up to 68 GPa. The data indicate that the orthorhombic (*Cmcm*) ambient-pressure phase ($K_0 = 154 \pm 22$ GPa with $K_0' = 5.2 \pm 0.5$) undergoes a first-order transition at 18 GPa to a new orthorhombic ($Pmc2_1$) structure. This new high-pressure polymorph remains stable up to 42 GPa, after which the emergence of a second high-pressure monoclinic ($P2_1/c$) phase is observed.

Introduction

A new titanium oxynitride phase, $Ti_{2.85}O_4N$, was recently discovered using the synthetic route of atmospheric pressure chemical vapor deposition combined with combinatorial materials exploration:[1] this new material was shown to be an active photocatalyst under UV illumination.[2] Chemical vapor deposition (CVD) is a technique more normally associated with thin film synthesis and industrial-scale deposition processes than with exploratory materials discovery research.[3] Recent studies conducted within the UCL group are now establishing the technique as a method for synthesizing new solid-state compounds and materials that may have technologically important properties, including photocatalysis. This work has focused recently on synthesis of novel semiconducting titanium oxynitride polymorphs that are poorly represented in the database at present. These are of primary interest for exploration because of the known optoelectronic and photocatalysis properties of TiO_2 and its N-doped equivalents, combined with predictions of new Ti_3N_4 and related oxynitrides based on ab initio theoretical studies combined with high-pressure−high-temperature synthesis studies.[4−6] Such new metal nitride and oxynitride compounds and their crystalline polymorphs are of great interest for development of new materials for photocatalysis, including water-splitting for energy applications, fine chemical production, and water decontamination and disinfection procedures.[7−9] Two main groups of titanium oxynitride materials have been investigated so far: first, TiO_xN_y phases that exist as a solid solution between the rock-salt structured end members TiN and TiO ($x + y \sim 1$) and N-doped TiO_2N_x phases, with the nitrogen doping <1−5%.[10,11] These latter materials have been identified as potential visible light photocatalysts.[12] Here, we have adopted the novel technique of using the CVD-synthesized material as a precursor for high-pressure studies to investigate the formation and recovery of new crystalline polymorphs. We predicted that this approach would result in higher-density titanium oxynitride structures with useful optoelectronic properties that could be developed for photocatalytic applications.[13,14]

The archetype Ti_3O_5 material for our investigations is a member of the Magnéli series of Ti_nO_{2n+1} phases with $n = 3$. It occurs at room temperature as an insulator with a monoclinic structure (β-Ti_3O_5). It undergoes a phase transition at 450 K to a second monoclinic structure (β') with a sharp 6% increase in unit cell volume. Further heating to 500 K leads to a second phase transition to the orthorhombic α-Ti_3O_5 structure.[15] The phase transition and volume increase at 450 K are associated with an insulator−metal transition. In the low T β phase, the titanium d electrons are localized within a metal−metal bond, which, above the transition temperature, become delocalized: breaking the metal−metal bond results in a relaxation of the structure and unit cell expansion. Previous work has found that reduction of the Fermi level by substituting Ti^{4+} with cations of lower charge causes a lowered transition T to be observed.[16−18] Hyett et al. demonstrated that a similar effect can be observed using anionic substitution in the new compound $Ti_{2.85}O_4N$ prepared by CVD, comparable with that achieved in α-Ti_3O_5 at $T > 500$ K.[1] High-pressure techniques provide a powerful tool for investigation of polymorphism and synthesis of new materials.[19] There have been a few previous studies of titanium oxides and nitrides under high-pressure conditions.[20,21] The polymorphism in TiO_2 has been investigated extensively, including studies of nanomaterials.[22−24] Åsbrink et al. investigated β-Ti_3O_5 (*C*2/*m* structure) up to 40 GPa but were unable to identify any pressure-induced phase transitions.[25] Here, we report high-pressure polymorphism of the new oxynitride compound $Ti_{2.85}O_4N$ using synchrotron X-ray diffraction techniques in a diamond anvil cell.

Experimental Techniques

A thin film of $Ti_{2.85}O_4N$ was synthesized via atmospheric pressure chemical vapor deposition (APCVD) from the reaction between gaseous titanium(IV) chloride, ethyl acetate, and ammonia deposited onto a glass surface. Titanium(IV) chloride (Aldrich, 99.9%) and ethyl acetate (Fisher, Reagent grade) were heated in bubblers to 82 and 39 °C, respectively, to generate vapors of these precursors, which were then transported to a mixing chamber with N_2 gas (BOC), with flow rates of 2 and 0.5 L min^{-1} through the titanium(IV) chloride and ethyl acetate, respectively. Ammonia vapor was transported to the mixing

* To whom correspondence should be addressed. E-mail: p.f.mcmillan@ucl.ac.uk (P.F.M.), i.p.parkin@ucl.ac.uk (I.P.P.).

10.1021/jp100769r
Published on Web 04/20/2010

chamber using its own room temperature vapor pressure. In the mixing chamber, the precursor gases were combined with a plain N_2 flow of 12 L min^{-1} and carried into the reaction chamber. All gas transport pipes and the mixing chamber were heated to 200 °C to avoid precursor condensation. The reaction chamber consisted of a 330 mm long silica tube with a diameter of 105 mm, containing a half-cylinder graphite block on which rested the glass substrate (220 × 90 × 3 mm^3). Whatman heater catridges inserted into the graphite block heated the substrate to 660 °C, at which temperature the precursors reacted to form a thin film of the titanium oxynitride. The deposition was conducted for 5 min. Additional details of the synthesis experiments along with chemical and structural characterization of the samples have been given previously.[1]

For high-pressure experiments, the thin film sample was removed from the substrate and ground into a powder. The $Ti_{2.85}O_4N$ material was precompressed between tungsten carbide cubes before being loaded into a cylindrical diamond anvil cell. Runs were carried out both nonhydrostatically without any pressure-transmitting medium and also using nitrogen cryogenically loaded into the DAC as a quasi-hydrostatic medium over at least part of the pressurization range. Experiments were carried out up to 68 GPa using 200 or 300 μm diamond culets. Rhenium gaskets were preindented to 30 μm and drilled using electroerosion to provide 80 μm holes. Pressure was determined using ruby fluorescence.[26] X-ray diffraction data were obtained at station ID27 of the European Synchrotron Radiation Facility (Grenoble, λ_0 = 0.3738 Å) and at beamline I15 at Diamond Light Source (Didcot, λ_0 = 0.4441 Å). At the ESRF, the 2 × 3 μm beam permitted micrometer-scale mapping of the sample chamber, whereas at Diamond, the incident beam was collimated to 30 μm. Two-dimensional diffraction data were recorded using either a CCD detector or a MAR 345 image plate and then integrated and transformed to 1-D patterns using Fit2D[27] and analyzed using GSAS,[28,29] FullProf,[30] and PowderCell.[31]

Results and Discussion

The composition of the starting $Ti_{2.85}O_4N$ sample produced by APCVD synthesis was determined previously using a combination of chemical analysis methods and Rietveld refinement of the powder X-ray synchrotron diffraction data.[1] A minor impurity peak at 2.52 Å identified as TiC represented <0.5% of the sample.

In a first series of high-pressure runs, we loaded the sample using N_2 as the pressure-transmitting medium and obtained high-quality data in the low-pressure range that we could analyze using refinement methods (Figure 1). Above 16−18 GPa, the data quality was reduced dramatically. We can partly associate this with the $\delta-\varepsilon$ transition of crystalline N_2.[32,33] However, a phase transition occurring in the $Ti_{2.85}O_4N$ sample was also indicated from the X-ray data in the same pressure range (Figure 2). We carried out a second series of runs with no pressure-transmitting medium present. This clearly showed the same transition occurring within the titanium oxynitride compound at around 18 GPa.

The X-ray diffraction data were analyzed using Le Bail methods to provide information on unit cell and d_{hkl} spacing variations with pressure (see Table 1).[34] These clearly identified contributions from the N_2 pressure-transmitting medium and the TiC impurity (Figure 1). The X-ray diffraction patterns of $Ti_{2.85}O_4N$ could be modeled using the ambient-pressure structure until ~14 GPa: above 18 GPa, the diffraction pattern first showed the emergence of a second orthorhombic phase mainly characterized by the appearance of a new peak at 11.6° 2θ. The

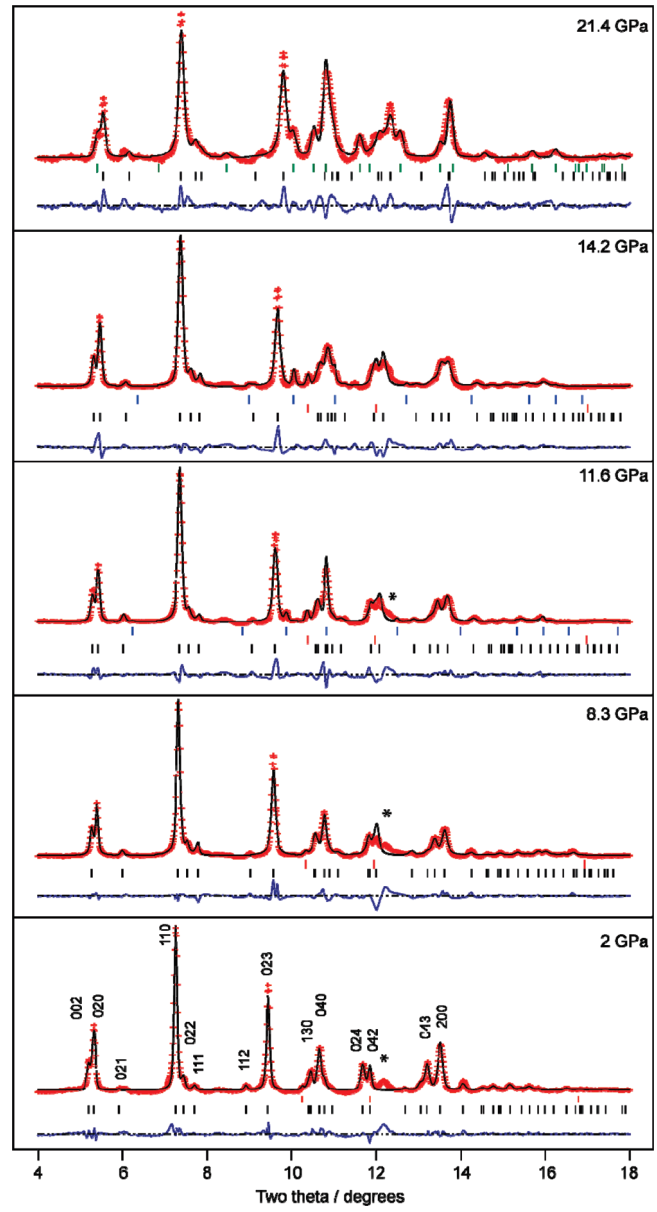

Figure 1. Le Bail refinements of diffraction data obtained up to 21.4 GPa in N_2 pressure-transmitting medium. Data points and Le Bail fits are overlaid in red and black, respectively, and difference plots are shown. The tick marks indicate peaks for the *Cmcm* $Ti_{2.85}O_4N$ structure (below), the high-pressure $Pmc2_1$ present at 21.4 GPa, and the TiC impurity and the δ- and ε-N_2 phases of the pressure medium. Asterisks (*) mark an identified broad peak that was assigned to an unknown impurity.

new structure could be refined within $Pmc2_1$ symmetry, based on systematic *hkl* absences. However, the low-pressure *Cmcm* phase could still be identified in the diffraction pattern until ~42 GPa, indicating that the transition must be first-order in nature. By 24 GPa, at least five peaks were observed due to the new high-pressure phase. These were indexed to an orthorhombic $Pmc2_1$ structure with a = 2.401 Å, b = 4.712 Å, and c = 6.019 Å (V = 68.10 $Å^3$) at a pressure of 24 GPa (see Table 2). This phase was found to be stable to beyond 42 GPa. By 68 GPa, at least two of the peaks develop shoulders, indicating a potential further phase change (Figure 3). Experiments conducted with no pressure-transmitting medium to above this pressure clearly revealed a potential second high-pressure phase transition. The second high-pressure phase is indexed as

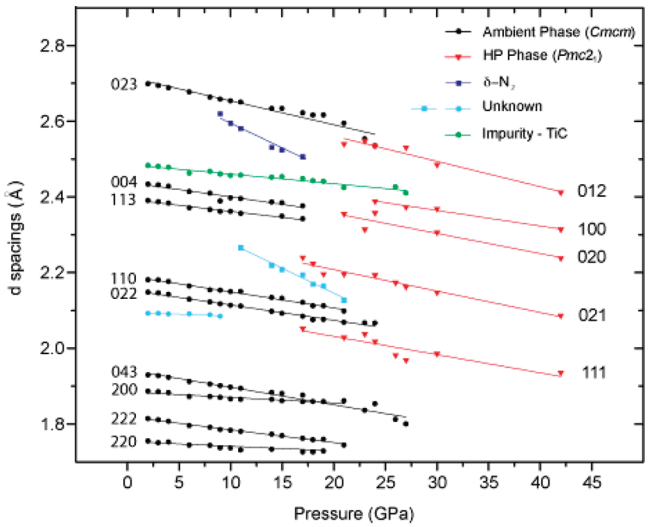

Figure 2. Positions recorded for diffraction peaks observed in the XRD data as a function of increasing pressure (GPa). The data indicate the appearance of a new phase (assigned by Le Bail refinement to $Pmc2_1$ symmetry) above 15−20 GPa. The low-pressure *Cmcm* phase persists to at least 23−27 GPa, indicating that the transformation is first-order. The d_{hkl} vs P data clearly reveal peaks due to e and δ phases of N_2 used as a pressure-transmitting medium as well as TiC and weak features due to an unidentified impurity phase.

TABLE 1: Cell Constants and Unit Cell Volume for $Ti_{2.85}O_4N$ (*Cmcm*) As Determined by Le Bail Refinement

pressure (GPa)	*a* (Å)	*b* (Å)	*c* (Å)	volume (Å^3)
2	3.7751(2)	9.577(1)	9.8053(8)	354.51(3)
3	3.7710(2)	9.5644(9)	9.7906(8)	353.12(3)
4	3.7636(3)	9.540(1)	9.767(1)	350.68(6)
5.3	3.7583(2)	9.520(1)	9.742(1)	348.53(5)
6.8	3.7474(3)	9.481(1)	9.730(1)	345.69(4)
8.3	3.7456(2)	9.455(1)	9.674(1)	342.58(4)
9.5	3.7364(3)	9.428(1)	9.665(1)	340.49(5)
10.2	3.7321(2)	9.409(1)	9.650(1)	338.84(5)
11.6	3.7272(2)	9.397(1)	7.638(1)	337.59(4)
12.4	3.7211(3)	9.373(2)	9.604(2)	334.95(7)
14.2	3.7207(3)	9.337(1)	9.585(1)	332.99(5)
15.6	3.7221(3)	9.325(1)	9.576(1)	332.39(5)
17.2	3.7156(4)	9.294(2)	9.530(2)	329.10(7)
18.4	3.7159(4)	9.268(2)	9.513(2)	327.63(7)
19.7	3.7149(5)	9.264(2)	9.499(2)	326.91(9)
21.4	3.7197(5)	9.190(2)	9.449(2)	323.0(1)
23.1	3.7245(5)	9.194(2)	9.442(2)	323.3(1)

TABLE 2: Cell Constants and Unit Cell Volume for the High-Pressure Phase of $Ti_{2.85}O_4N$ ($Pmc2_1$) As Determined by Le Bail Refinement

pressure (GPa)	*a* (Å)	*b* (Å)	*c* (Å)	volume (Å^3)
19	2.446(1)	4.799(1)	6.107(1)	71.686(3)
21.4	2.422(1)	4.714(1)	6.022(1)	68.755(3)
23.1	2.41(1)	4.692(1)	6.023(1)	68.106(3)
24	2.401(1)	4.712(1)	6.019(1)	68.096(3)
30	2.371(1)	4.612(1)	5.906(1)	64.582(3)
42	2.315(1)	4.481(1)	5.735(1)	59.492(3)

monoclinic ($P2_1/c$), corresponding to a distortion of the orthorhombic $Pmc2_1$ high-pressure phase. Le Bail analysis indicates $a = 4.3456(5)$ Å, $b = 5.177(3)$ Å, $c = 2.872(1)$ Å, and $\beta = 99.7(1)°$ at $P = 68$ GPa.

Figure 4 shows the variation of lattice parameters of $Ti_{2.85}O_4N$ structures during compression, beginning with the ambient T

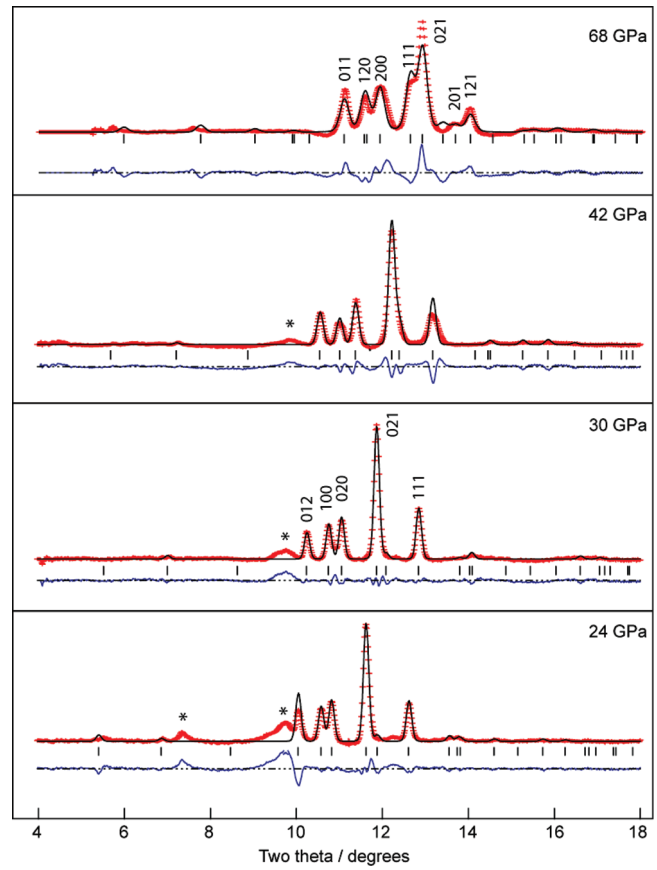

Figure 3. Nonhydrostatic compression data obtained with no pressure-transmitting medium at 24, 30, 42, and 68 GPa. The Le Bail refined X-ray diffraction patterns are of the $Pmc2_1$ high-pressure phase of $Ti_{2.85}O_4N$. Asterisks (∗) mark peaks resulting from remaining contributions from the ambient-pressure *Cmcm* phase. At 68 GPa, additional contributions indicating a second transformation into a monoclinic ($P2_1/c$) phase are observed.

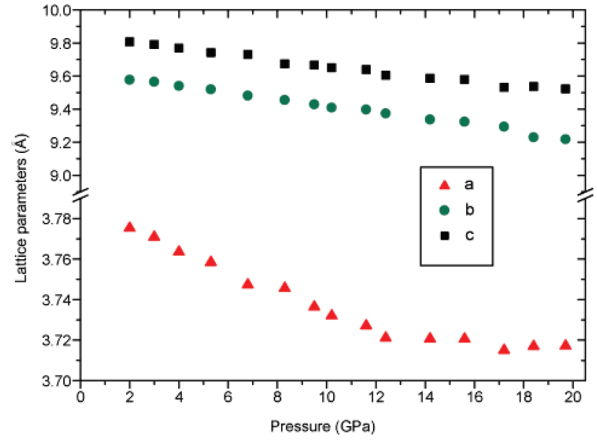

Figure 4. Plot of lattice parameters for the low- and high-pressure phases of $Ti_{2.85}O_4N$. The *a*, *b*, and *c* lattice parameters (Å) for the ambient phase of Ti_3O_4N (*Cmcm*) against pressure (GPa) are reported. The lattice parameters were determined using Le Bail refinement and are plotted with their corresponding *y* axis.

structure prepared by APCVD. The *b* and *c* parameters show an approximately linear decrease with pressure, corresponding to a 4% shortening in these parameters at a pressure of 20 GPa. However, *a* behaves differently: the initial compression is much lower (∼1%) and it completely ceases at ∼12 GPa. Interestingly, the same effect was observed previously for the monoclinic

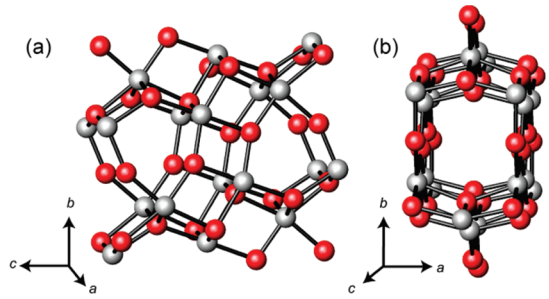

Figure 5. Representation of the unit cell of $Ti_{2.85}O_4N$, showing the titanium ions (gray) and anion sites (red). View of the (a) 100 face and (b) 001 face. From this can be seen the three coordinate anion sites between the tense titania layers that allow the relatively higher compressibility in the *b* and *c* directions.

β-Ti_3O_5 phase,[25] indicating that it does not depend on the presence of Ti vacancies or the degree of O/N substitution. In the case of Ti_3O_5, the *a* axis was found to have a linear compression of 0.8% that ceased at ~10 GPa compared with 6.7 and 5.4% for the *b* and *c* axes across the entire range up to 38 GPa. In both β-Ti_3O_5 and $Ti_{2.85}O_4N$ (Figure 5), the noticeably stiffer lattice direction is associated with dense columns of distorted edge-sharing TiO_6 octahedra along the 100 direction. These highly constrained structures have little possibility for angular distortion, and the linked Ti−O bonds resist compression along the axis. By 10−12 GPa, the maximum compressibility limit of the $(TiO_6)_n$ chains has been reached. The polyhedral compressibility for unlinked TiO_6 octahedra was estimated to be $\Delta V/V_o \sim 0.04$ GPa^{-1}, giving a maximum Ti−O bond compression at 10 GPa of ~1.5%. Along the 010 and 001 directions, the dense layers are interconnected by three coordinate anion sites that allow greater angular flexibility and, thus, the larger compressibility values recorded for the *b* and *c* dimensions over the entire pressure range, with no compression limit observed in the 10−12 GPa range. This observation indicates that the Ti_3O_5 and $Ti_{2.85}O_4N$ materials constitute remarkably rigid structures along one crystallographic direction.

The *V*(*P*) data were used to estimate the bulk modulus and its pressure derivative for the ambient-pressure $Ti_{2.85}O_4N$ compound as well as the new high-pressure phase. The compression data were analyzed using a finite strain Birch−Murnaghan equation of state (EOS) expression expanded to third order and the K_0 and K_0' values refined by constructing an Eulerian finite-strain reduced variable *F*−*f* plot (Figure 6).[35] The data indicate a bulk modulus of $K_0 = 154 \pm 22$ GPa with $K_0' = 5.2 \pm 0.5$ for the ambient-pressure *Cmcm* phase of $Ti_{2.85}O_4N$. This is slightly lower than that obtained for β-Ti_3O_5 ($K_0 = 173$ GPa[25]) that can be attributed to the presence of cation vacancies in the oxynitride structure.

Recovery of the high-pressure phase to ambient conditions was studied during decompression from above 27 GPa, where the presence of the ambient phase was minimized in the X-ray diffraction pattern. The diffraction pattern of the high-pressure phase ($Pmc2_1$) is clearly visible during the first two pressure steps down to 25 GPa (Figure 7). Here, we have superposed the diffraction pattern obtained at 24 GPa for comparison. The peaks that are quite broad could indicate inhomogeneous strains present within the sample or structural disordering or even a nanocrystalline state. Although all of the diffraction peaks can be identified, there are marked changes in relative intensities between pressure points that could be due to changes in crystallite orientation relative to the incident beam. By 20 GPa, the main diffraction peaks become further broadened and new

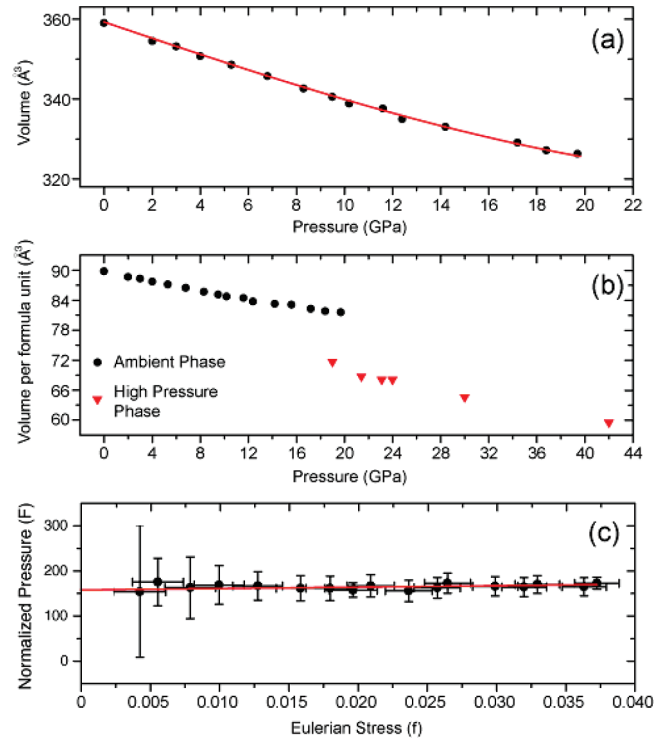

Figure 6. (a) A *V*(*P*) plot of compression data for the *Cmcm* phase of $Ti_{2.85}O_4N$. A Birch−Murnaghan equation of state reduced to the third order is fitted to the single phase. (b) The volume per formula unit is plotted as a function of pressure. A discontinuity is observed between the ambient phase (*Cmcm*) of $Ti_{2.85}O_4N$ and that of the first high-pressure phase ($Pmc2_1$). (c) Normalized pressure (*F*) vs Eulerian strain (*f*).

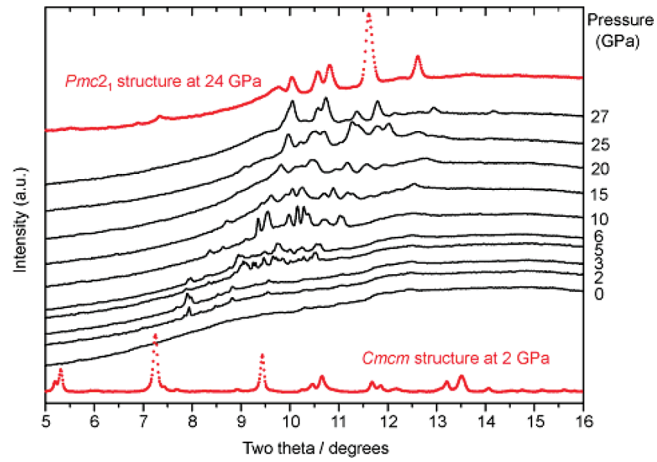

Figure 7. X-ray diffraction patterns of the decompression of the high-pressure phase of Ti_3O_4N from 27 to 0 GPa. Patterns shown in red are for reference and from the compression data sets at 2 and 24 GPa showing the patterns of the ambient structure and high-pressure structure, respectively.

features begin to appear in the pattern. At 15 GPa, below the first-order transition observed during the compression run, the broad diffraction peaks of the high-pressure phase can still be discerned in the pattern, but now a series of additional sharper peaks are clearly present that become better defined as the pressure is lowered to 10 GPa (Figure 7). A further new set of peaks is observed in the 5−6 GPa region that disappear by 2−3 GPa to be replaced by a simple peak pattern superimposed on a broad amorphous background. None of these series of peaks

correspond to structures identified within the $Ti_xO_yN_z$ system to date, and they likely correspond to metastable phases occurring as the highly metastable high-density $Ti_{2.85}O_4N$ structure is decompressed beyond its low-pressure stability limit. Upon complete decompression to a pressure of 1 atm, only weak broad bands indicating an amorphous or high disordered nanocrystalline material remain in the pattern. The results indicate that, following its formation at high pressure, the orthorhombic $Pmc2_1$ phase is not recoverable to ambient conditions, and decompression in the diamond anvil cell at room temperature results in recovery of amorphous material. We also carried out preliminary experiments using a multianvil apparatus, heating the $Ti_{2.85}O_4N$ at a pressure greater than 20 GPa to attempt to obtain a better crystallized sample that might be recoverable to ambient conditions. However, all of these investigations resulted in formation of a mixture of TiO_2 and TiN that is likely to be thermodynamically stable under the high-pressure−high-temperature conditions.

Conclusion

An investigation of the high-pressure behavior of $Ti_{2.85}O_4N$ was carried out using a diamond anvil cell and with synchrotron X-ray powder diffraction techniques. The diffraction pattern of the ambient-pressure *Cmcm* phase could be analyzed up to a pressure of 20 GPa to study its compressional behavior. The *b*- and *c*-axis parameters showed a near-linear decrease throughout the pressure range. The *a* parameter had a much smaller compressibility, and this stopped above 12 GPa. This behavior is similar to that of β-Ti_3O_5, and it can be explained by the relative incompressibility of edge-sharing chains of TiO_6 octahedra along the (100) direction.[36] The appearance of a new phase is indicated in the diffraction data above 18 GPa. The new compound can be indexed as an orthorhombic $Pmc2_1$ structure. However, the ambient-pressure *Cmcm* phase can still be recognized in the diffraction pattern up to a pressure of 42 GPa, indicating that the transition is first-order. The compressibility parameters of the two phases were analyzed using a third-order Birch−Murnaghan equation of state. Further compression to above 65 GPa indicates a further transition into a phase with $P2_1/c$ symmetry. During decompression experiments, the $Pmc2_1$ phase was not recoverable to 1 atm. At least three new metastable crystalline phases were observed to occur during decompression that have not yet been identified. The material recovered to ambient conditions was amorphous. High-pressure, high-temperature synthesis experiments resulted in transformation of the material into a mixture of TiO_2 and TiN phases that are thermodynamically stable under these conditions.

Acknowledgment. This work was supported by EPSRC Portfolio Grant EP/D504782 and a Senior Research Fellowship (EP/D07357X) to P.F.M. G.H. thanks the Ramsay Memorial Trust for a research fellowship, and I.P.P. is a Wolfson-Royal Society Research Merit Award fellow. We thank Nicholas A. Spencer, Edward Bailey, and Rachael Hazael for assistance with high-pressure synthesis and synchrotron experiments.

References and Notes

(1) Hyett, G.; Green, M. A.; Parkin, I. P. The use of combinatorial chemical vapor deposition in the synthesis of Ti_3-δO_4N with $0.06 < \delta < 0.25$: A titanium oxynitride phase isostructural to anosovite. *J. Am. Chem. Soc.* **2007**, *129*, 15541.

(2) Hyett, G.; Green, M. A.; Parkin, I. P. Ultra-violet light activated photocatalysis in thin films of the titanium oxynitride, Ti_3-δO_4N. *J. Photochem. Photobiol., A* **2009**, *203*, 199.

(3) Choy, K. L. Chemical vapour deposition of coatings. *Prog. Mater. Sci.* **2003**, *48*, 57.

(4) Kroll, P. Hafnium nitride with thorium phosphide structure: Physical properties and an assessment of the Hf-N, Zr-N, and Ti-N phase diagrams at high pressures and temperatures. *Phys. Rev. Lett.* **2003**, *90*, 4.

(5) Zerr, A.; Miehe, G.; Serghiou, G.; Schwarz, M.; Kroke, E.; Riedel, R.; Fuess, H.; Kroll, P.; Boehler, R. Synthesis of cubic silicon nitride. *Nature* **1999**, *400*, 340.

(6) Zerr, A.; Miehe, G.; Riedel, R. Synthesis of cubic zirconium and hafnium nitride having Th_3P_4 structure. *Nat. Mater.* **2003**, *2*, 185.

(7) Maeda, K.; Domen, K. New non-oxide photocatalysts designed for overall water splitting under visible light. *J. Phys. Chem. C* **2007**, *111*, 7851.

(8) Sato, J.; Saito, N.; Yamada, Y.; Maeda, K.; Takata, T.; Kondo, J. N.; Hara, M.; Kobayashi, H.; Domen, K.; Inoue, Y. RuO_2-loaded β-Ge_3N_4 as a non-oxide photocatalyst for overall water splitting. *J. Am. Chem. Soc.* **2005**, *127*, 4150.

(9) Ebbinghaus, S. G.; Abicht, H.-P.; Dronskowski, R.; Mller, T.; Reller, A.; Weidenkaff, A. Perovskite-related oxynitrides - Recent developments in synthesis, characterisation and investigations of physical properties. *Prog. Solid State Chem.* **2009**, *37*, 173.

(10) Dunnill, C. W.; Parkin, I. P. N-doped titania thin films prepared by atmospheric pressure CVD using *t*-butylamine as the nitrogen source: Enhanced photocatalytic activity under visible light. *Chem. Vap. Deposition* **2009**, *15*, 171.

(11) Morikawa, T.; Asahi, R.; Ohwaki, T.; Aoki, K.; Taga, Y. Band-gap narrowing of titanium dioxide by nitrogen doping. *Jpn. J. Appl. Phys., Part 2* **2001**, *40*, L561.

(12) Kuroda, Y.; Mori, T.; Yagi, K.; Makihata, N.; Kawahara, Y.; Nagao, M.; Kittaka, S. Preparation of visible-light-responsive $TiO_{2-x}N_x$ photocatalyst by a sol−gel method: Analysis of the active center on TiO_2 that reacts with NH_3. *Langmuir* **2005**, *21*, 8026.

(13) Lowther, J. E. Metal oxides. *MRS Bull.* **2003**, *28*, 189.

(14) Dubrovinsky, L. S.; Dubrovinskaia, N. A.; Swamy, V.; Muscat, J.; Harrison, N. M.; Ahuja, R.; Holm, B.; Johansson, B. Metal oxides. *Nature* **2001**, *410*, 653.

(15) Onoda, M. Phase transitions of Ti_3O_5. *J. Solid State Chem.* **1998**, *136*, 67.

(16) Grey, I. E.; Li, C.; Madsen, I. C. Phase-equilibria and structural studies on the solid-solution $MgTi_2O_5$-Ti_3O_5. *J. Solid State Chem.* **1994**, *113*, 62–73.

(17) Grey, I. E.; Ward, J. X-ray and Mossbauer study of $FeTi_2O_5$-Ti_3O_5 system. *J. Solid State Chem.* **1973**, *7*, 300.

(18) Kellerman, D. G.; Zhilyaev, V. A.; Perelyaev, V. A.; Shveikin, G. P. Effect of doping on the phase-transition in Ti_3O_5. *Inorg. Mater.* **1983**, *19*, 221–224.

(19) Schettino, V.; Bini, R. Constraining molecules at the closest approach: Chemistry at high pressure. *Chem. Soc. Rev.* **2007**, *36*, 869.

(20) Mattesini, M.; de Almeida, J. S.; Dubrovinsky, L.; Dubrovinskaia, N.; Johansson, B.; Ahuja, R. High-pressure and high-temperature synthesis of the cubic TiO_2 polymorph. *Phys. Rev. B* **2004**, *70*, 4.

(21) Muscat, J.; Swamy, V.; Harrison, N. M. First-principles calculations of the phase stability of TiO_2. *Phys. Rev. B* **2002**, *65*, 15.

(22) Jamieson, J. C.; Olinger, B. High-pressure polymorphism of titanium dioxide. *Science* **1968**, *161*, 893.

(23) Zhang, W. F.; He, Y. L.; Zhang, M. S.; Yin, Z.; Chen, Q. Raman scattering study on anatase TiO_2 nanocrystals. *J. Phys. D: Appl. Phys.* **2000**, *33*, 912.

(24) Swamy, V.; Kuznetsov, A.; Dubrovinsky, L. S.; McMillan, P. F.; Prakapenka, V. B.; Shen, G.; Muddle, B. C. Size-dependent pressure-induced amorphization in nanoscale TiO_2. *Phys. Rev. Lett.* **2006**, *96*, 4.

(25) Asbrink, S.; Gerward, L.; Olsen, J. S. A high-pressure study of Ti_3O_5 by X-ray diffraction and synchrotron radiation. Pressures up to 38.6 GPa. *J. Appl. Crystallogr.* **1989**, *22*, 119.

(26) Mao, H. K.; Bell, P. M.; Shaner, J. W.; Steinberg, D. J. Specific volume measurements of Cu, Mo, Pd and Ag and calibration of ruby R1 fluorescence pressure gauge from 0.06 to 1 MBar. *J. Appl. Phys.* **1978**, *49*, 3276.

(27) Hammersley, A. P.; Svensson, S. O.; Hanfland, M.; Fitch, A. N.; Hausermann, D. Fit2D. *High Pressure Res.* **1996**, *14*, 235.

(28) Larson, A. C.; Dreele, R. B. V. General Structure Analysis System (GSAS). *Los Alamos National Laboratory Report LAUR 86-748*; Los Alamos National Laboratory: Los Alamos, NM, 2000.

(29) Toby, B. H. EXPGUI for GSAS. *J. Appl. Crystallogr.* **2001**, *34*, 210.

(30) Rodriguez-Carvajal, J. FullProf98 and WinPLOTR. *Physica B* **1993**, *192*, 55.

(31) Kraus, W.; Nolze, G. PowderCell software. *J. Appl. Crystallogr.* **1996**, *29*, 301–303.

(32) Schiferl, D.; Buchsbaum, S.; Mills, R. L. Phase-transitions in nitrogen observed by Raman spectroscopy from 0.4 to 27.4 GPa at 15 K. *J. Phys. Chem.* **1985**, *89*, 2324.

(33) Bini, R.; Ulivi, L.; Kreutz, J.; Jodl, H. J. High-pressure phases of solid nitrogen by Raman and infrared spectroscopy. *J. Chem. Phys.* **2000**, *112*, 8522.

(34) Bail, A. L.; Duroy, H.; Fourquet, J. L. Ab-initio structure determination of $LiSbWO_6$ by X-ray powder diffraction. *Mater. Res. Bull.* **1988**, *23*, 447.

(35) Salamat, A.; Woodhead, K.; McMillan, P. F.; Cabrera, R. Q.; Rahman, A.; Adriaens, D.; Cora, F.; Perrillat, J. P. Tetrahedrally bonded dense C_2N_3H with a defective wurtzite structure: X-ray diffraction and Raman scattering results at high pressure and ambient conditions. *Phys. Rev. B* **2009**, *80*, 104106.

(36) Hazen, R. M.; Finger, L. W. Bulk modulus-volume relationship for cation-anion polyhedra. *J. Geophys. Res.* **1979**, *84*, 6723.

JP100769R